atmosphere

MDPI

Article

Thermal and Dynamical Characteristics of Landfalling Severe Typhoons in South China against Different Monsoon Backgrounds

Zhixiang Xiao [1,2] and Cai Yao [2,3,*]

[1] School of Geography and Planning, Nanning Normal University, Nanning 530001, China
[2] Guangxi Institute of Meteorological Sciences, Nanning 530022, China
[3] Southern Marine Science and Engineering Guangdong Laboratory (Zhuhai), Zhuhai 519000, China
* Correspondence: gxyaocai@126.com

Abstract: The characteristics of landfalling severe typhoons (LSTYs)—i.e., typhoons with landfall intensities of 2 min with a mean maximum sustained wind $\geq$41.5 m s^{-1}—in South China (SC) were here examined. Thirteen LSTYs have been recorded in SC since 1949, and most of them underwent a rapid intensification before landfall. The LSTYs were classified into three categories based on the intensity of the western North Pacific summer monsoon, i.e., as weak, moderate, and strong monsoons. The characteristics of the three types of LSTYs are markedly different. Two LSTYs (7317 and 1523) were developed against a weak monsoon (WM) background and did not have abundant monsoon water vapor drawn into the typhoon cores. Therefore, these two LSTYs exhibited smaller horizontal outer sizes and weaker "warm–wet" cores than those in moderate and strong monsoons. However, a warm offshore ocean supplied a sufficient amount of energy, favoring these two LSTYs' rapid intensification before landfall. There have been five LSTYs (9113, 0518, 0816, 1320, and 1826) that formed under strong monsoon (SM) conditions but obtained a poor energy supply from the coastal ocean. Embedded in the SM, the vigorous warm–wet monsoon flow was drawn into the typhoons and persisted for several days until landfall. Then, the five LSTYs developed strongly at the greatest horizontal scale and were maintained as severe typhoons for almost 48 h before landfall. The beneficial warm–wet atmospheric circulation stimulated the strongest warm (wet) core at the upper (lower) level of the LSTYs, and a secondary, low-level warm core occurred as well. In moderate monsoon (MM) cases (8106, 9617, 1311, 1410, 1418, and 1714), the strength of the monsoon flow, the "warm–wet" core of the typhoon, and the ocean energy supply were ranked just between those of the LSTYs in WMs and SMs. The development of the LSTYs in the MM cases resulted from a combination of the effects of monsoon and ocean energy supply. In addition, the powerful upper-level divergence ascribed to the strong South Asia High may have played an auxiliary role in MM cases. From the perspective of the sea surface temperature (SST) response to the LSTYs, because of a relatively fast translation speed and the warmer subsurface ocean, the SST cooling was weakest for WM cases. However, the strongest SST cooling was found in SM cases and it was partially due to their slowest translation speed.

Keywords: landfalling severe typhoons; South China; monsoon; SST

check for updates

Citation: Xiao, Z.; Yao, C. Thermal and Dynamical Characteristics of Landfalling Severe Typhoons in South China against Different Monsoon Backgrounds. *Atmosphere* **2023**, *14*, 338. https://doi.org/10.3390/atmos14020338

Academic Editors: Chundi Hu and Han Zhang

Received: 28 December 2022
Revised: 28 January 2023
Accepted: 2 February 2023
Published: 8 February 2023

Copyright: © 2023 by the authors. Licensee MDPI, Basel, Switzerland. This article is an open access article distributed under the terms and conditions of the Creative Commons Attribution (CC BY) license (https://creativecommons.org/licenses/by/4.0/).

1. Introduction

Tropical cyclones (TCs) are one of the most high-impact destructive weather systems around the world, especially for coastal residents, due to the strong winds, torrential rains, storm surges, and landslides [1]. Tropical Cyclone Nargis crossed over southern Myanmar in May 2008, destroying large buildings, farmlands, and infrastructure, leading to the loss of more than 130,000 lives [2]. Generally, stronger TCs cause a greater damage to property and losses of life [3–5]. Catastrophic destruction has been caused by supertyphoons—e.g., Haiyan (2013), Rammasun (2014), and Lekima (2019)—in the Philippines and China [6–8],

resulting in heavy tolls on life and property [9,10]. In the warmer future climate, numerical simulations show that the intensity and frequency of intense TCs will continue to increase [11,12]. Stronger TCs will sustain longer and penetrate farther inland [13], and not only coastal citizens but also more inland populations will be threatened by severe TCs.

China is one of the countries most severely affected by TCs, and South China has the highest occurrence of landfalling TCs around the world [14]. TC landfall intensity has been investigated extensively. Liu and Chan [15] found that the intensity of TCs in South China (SC) has significantly increased and claimed that low vertical wind shear is one of the atmospheric factors. The increased landfall intensity is mainly caused by unprecedented increase in the TC intensification rate [16,17], which is largely due to the warming of the upper ocean and the sea surface temperature (SST) response to climate change [16–18]. The abovementioned studies mainly focused on basin-scale TCs, and relatively few studies have been conducted on regional landfalling severe typhoons (LSTYs); i.e., TCs with landfall intensities of a 2 min mean maximum sustained wind (MSW) $\geq$41.5 m s^{-1}. Recently, Yao et al. [18] found that more than 70% of the LSTYs in SC occurred after 2004, indicating the SC is facing more and more fearful threats from severe typhoons.

Monsoons are one of the important climate systems strongly interacting with typhoons. There is a high probability of an interaction between a typhoon and monsoon surge [19]. Monsoon gyres strongly modulate typhoons' intensity, tracks, and formation [20,21]. Interactions between landfalling typhoon precipitation and monsoon strength have been extensively investigated in previous studies [22–25]. Monsoon flow provides favorable conditions and abundant water vapor and energy to typhoons. Therefore, the monsoon flow does far more than simply modulate typhoon precipitation. Typhoon landfall intensity is also closely related to monsoon strength. A schematic of how a monsoon surge affected the landfall intensity of Supertyphoon Rammasun (1410) was depicted by Xiao et al. [26]. The low-frequency monsoonal water vapor transportation provided favorable conditions for the offshore enhancement of Rammasun [27]. Chen et al. [28] found that interactions between monsoon circulation and storm-scale vorticity anomalies were crucial for the rapid intensification of Typhoon Vicente (2012). The abovementioned work focused on case studies, and systematic research on the dynamic variation characteristics of extreme landfall typhoons in SC in relation to monsoons is absent. How LSTYs develop before landfall is an interesting question, especially during 0–72 h before landfall. Knowing the dynamic variation in LSTYs before landfall can help forecasters predict the TC landfall intensity, which is also beneficial for preventing disasters and reducing the effects on coastal citizens.

The goal of this study is to determine the similarities and differences in the LSTYs before they made landfall in SC against different monsoon backgrounds. The remainder of this paper is organized as follows. The data and methodology used are presented in Section 2. Section 3 provides information on LSTYs and their classification. A composite analysis of the LSTYs in terms of their environmental circulation and ocean conditions is undertaken in Section 4. Conclusions and a discussion are provided in Section 5.

2. Data and Methodology

2.1. Data

In this study, the TC best track data (1949–2021) were obtained from the Shanghai Typhoon Institute of China Meteorological Administration (STI/CMA), which provided the TC location and intensity at 6 h intervals (https://tcdata.typhoon.org.cn/en/index.html (accessed on 8 August 2022)). Each TC making landfall in China was recorded with detailed landfall information, such as the TCs name, landfall time, location, and intensity.

The large-scale atmospheric circulation was examined by using the fifth-generation global atmospheric reanalysis dataset (ERA5) [29] from the European Centre for Medium-Range Weather Forecasts (ECMWF) on 1.0° × 1.0° grids every 6 h. The version 3 daily Objectively Analyzed Air–Sea Fluxes (OAFlux) reanalysis products (1985–2021) from the Woods Hole Oceanographic Institution (WHOI) gridded at 1.0° × 1.0° were employed

here for air–sea interaction analysis, including sensible heat flux (SHF) and latent heat flux (LHF). Additionally, the daily-mean Optimum Interpolation Sea Surface Temperature (OISST) [30] with the horizontal resolution of 0.25° × 0.25° was also used.

2.2. Methodology

A dynamic composite analysis proposed by Gray et al. [31] and Li et al. [32] was used here to obtain the TCs' main features during its lifetime, i.e.,

$$\bar{S}_t(x,y) = \frac{1}{N}\sum_{n=1}^{N} S_t(x,y) \quad (1)$$

$S_t(x,y)$ is the variable at time t, $\bar{S}_t(x,y)$ is the sample average, and (x,y) is the coordinate of the selected region. The typhoon center at a specific time t is served as the origin coordinate. Then, $\bar{S}_t(x,y)$ is obtained by the averaged N samples for each grid point of (x,y).

Variation in the western North Pacific summer monsoon (WNPSM) is strongly coupled with cross-equatorial flows, the WNP monsoon trough, and the WNP subtropical high [33]. These systems are also closely associated with the landfall TCs in SC. In order to quantify the intensity of the WNPSM, the WNPSM index (WNPSMI) was selected for this study. It is defined as the difference in the 850 hPa zonal wind between a southern region and a northern region, i.e., $U_{850}(5^{o}-15^{o}\,\mathrm{N}, 100^{o}-130^{o}\,\mathrm{E}) - U_{850}(20^{o}-30^{o}\,\mathrm{N}, 110^{o}-140^{o}\,\mathrm{E})$. TCs are closely embedded in the WNPSM system and the mutual interactions between them are strong. In order to extract background environment circulation and minimize the TCs impact on calculating WNPSMI, the synoptic scale circulation is filtered out by the Lanczos filter method [34] and the remaining circulation is regarded as unaffected by typhoons. A larger WNPSMI calculated by the filtering wind fields indicates that a TC develops under a stronger monsoon background and a stronger southwesterly monsoon flow is drawn into TCs.

SST cooling is one of the most striking oceanic phenomena induced by TCs. A TC cools the SST and the cooling SST reduces the heat fluxes supplied to the typhoon, which affects the intensity of the typhoon. Thus, the cooling of SST induced by typhoons has been evaluated by the grid-based maximum response (GMR) method proposed by Li et al. [35].

3. The LSTYs in SC and Their Classification

3.1. The LSTYs in SC

There are more than 360 TCs making landfall in SC during 1949–2021. However, there are only thirteen LSTYs which have been recorded, as listed in Table 1, in order of the landfall (LF) intensity. It is worth noting that none of the LSTYs were found before 1973, which may be partially ascribed to the low data quality [36]. However, it is clear that most of them took place after 2004, as pointed out by Yao et al. [18]. Almost all of the LSTYs made landfall in SC in Jul–Aug–Sep (JAS), except Mujigae (1523), which was in October. The most intense landfall typhoon was Rammasun (1410), with the maximum MSW of ~70 m/s and the lowest central sea level pressure of 890 hPa. Only three of them (i.e., Rammasun, Marge, and Mujigae) maintain the grade SSTY when making landfall in SC.

The tracks of the LSTYs in SC are usually steady and from the southeast to northwest across SC (Figure 1a). As for the intensity (Figure 1b), only five (0816, 1311, 1320, 1410, and 1826) of them reached the level of being an STY before entering the South China Sea (SCS). The remaining eight LSTYs rapidly or slowly enhanced after entering the SCS and then intensified as STYs before landing in SC. The rapid intensification (RI) of the TCs used here is defined as Wang and Zhou [37], using the following criteria: the increase in the MSW reaches at least 2.5 m s^{-1}, 5 m s^{-1}, and 15 m s^{-1} in the first 6 h, 12 h, and 24 h, respectively. We find ten of the LSTYs experiencing at least one RI process before landfall, including five (7317, 8106, 0518, 1523, and 1714) of them which experienced RI in the SCS and four (9617,

1311, 1320, and 1826) which occurred to the east of 120° E. Whereas Rammasun (1410) was unique, it experienced two RI processes before making landfall in the Philippines and SC, leading to an unprecedented landfall intensity (70 m s^{-1}) in SC.

Table 1. The LSTYs in SC during 1949–2021.

Number	Name	LF Month	LF Province	LF Intensity (m/s)	LF Intensity (hPa)
1410	Rammasun	Jul	Hainan	70	890
7317	Marge	Sep	Hainan	60	925
1523	Mujigae	Oct	Guangdong	52	935
9617	Sally	Sep	Guangdong	50	935
0816	Hagupit	Sep	Guangdong	48	945
1714	Hato	Aug	Guangdong	48	945
8106	Kelly	Jul	Hainan	45	965
9113	Fred	Aug	Guangdong	45	960
0518	Damrcy	Sep	Hainan	45	950
1320	Usagi	Sep	Guangdong	45	930
1826	Mangkhut	Sep	Guangdong	45	955
1311	Utor	Aug	Guangdong	42	955
1418	Kalmaegi	Sep	Hainan	42	960

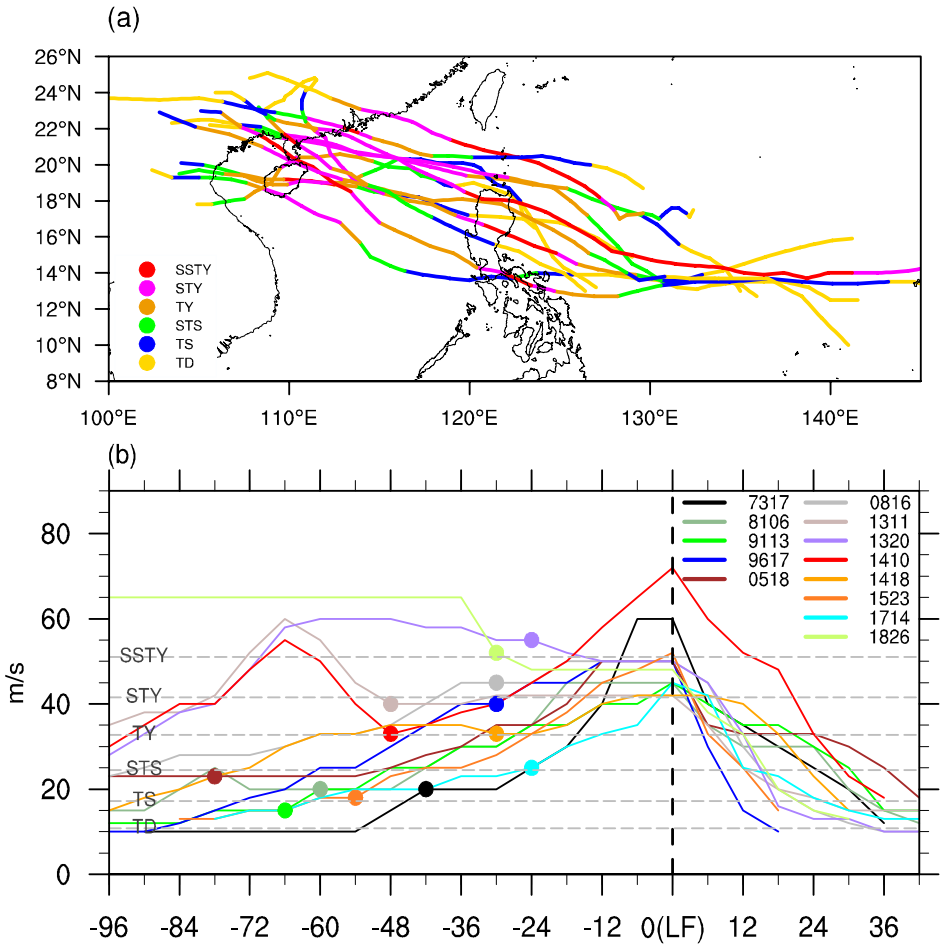


Figure 1. Tracks (**a**) and temporal variations in the intensity (**b**, units: m s^{-1}) of the 13 LSTYs in SC with 6 h intervals from 96 h before landfall (LF) to 42 h after LF. The vertical dash line and solid circles in (**b**) indicate the landfall time and the time of the LSTYs move into the SCS (west of 120° E), respectively.

3.2. Classification of the LSTYs

As shown in Figure 2a, the WNPSMI continued to enhance before the TCs making landfall in SC for all landfall TCs. The WNPSMI shows the most dramatic increasing trend during the LSTYs. Additionally, the intensification signal is found even seven days before the LSTYs landfall, i.e., the weakest WNPSMI was on day −7 and the strongest index was on day −1 (Figure 2a). Therefore, in order to investigate the monsoon's long-term impact on the LSTYs, the seven-day period, from day −7 to day 0 (LF), rather than a random day, is used here.

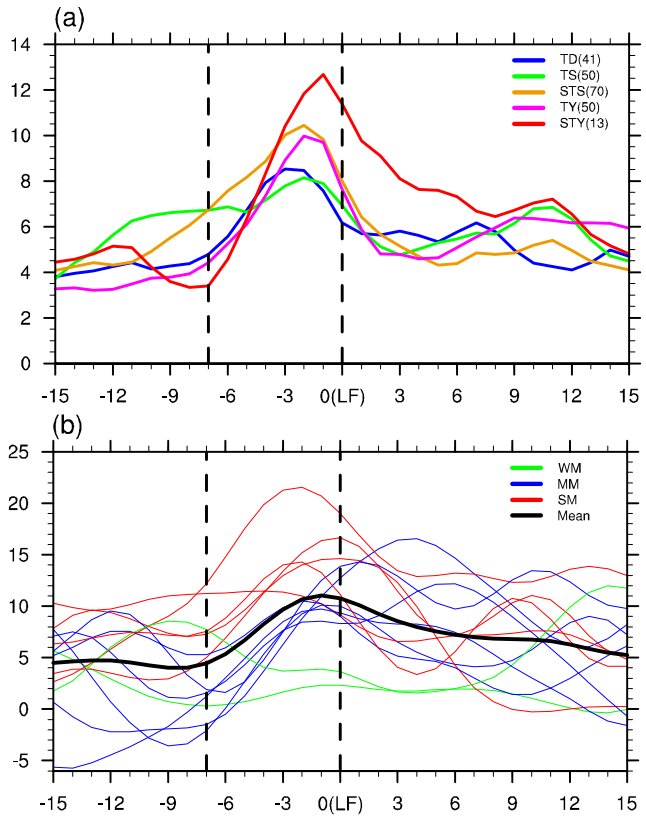


Figure 2. Time series of the WNPSMI fifteen days before (negative) and after (positive) TCs making landfall (LF) in SC. (**a**) The averaged WNPSMI for each type of landfall TCs. (**b**) The WNPSMI for each LSTYs and their mean values (black line), calculated by wind fields without TC circulation. The vertical dash lines indicate the landfall day and seven days (−7) prior to LF, respectively. Label legends in (**a**) indicate the landfall intensity in SC with the corresponding numbers of TCs in bracket.

The TCs' circulation strongly interacts with the background environment. Thus, the background circulation is extracted by the Lanczos filter method when calculating the WNPSMI (Figure 2b). It is worth noting that the WNPSMI shows little change whether the TCs' circulation is removed or not, except becoming smoother and slightly weakened (figure not shown). The result indicates that TCs' circulation has little impact on the background monsoon circulation. Though the unanimous enhancement of the WNPSMI for the landfall TCs is detected (Figure 2a), the temporal evolutions of the WNPSMI for each LSTY are diverse (Figure 2b). There is a big difference (~20 m s^{-1}) between the strongest and weakest monsoon index during the seven-day period before the TCs landfall. That is to say, the energy and water vapor transported from the monsoon flow to the LSTYs is totally different. It is interesting that the LSTYs intensified in such huge different monsoon backgrounds, but all of them made landfall with the intensity of an STY. The LSTYs have been divided into three clusters, i.e., a weak monsoon (WM; 7317 and 1523), moderate monsoon (MM; 8106, 9617, 1311, 1410, 1418, and 1714), and strong monsoon (SM; 9113,

0518, 0816, 1320, 1826), by a K-means clustering algorithm [38] according to the WNPSMI seven to zero days before landfall.

In the WM cluster, two LSTYs are embedded in inactive, weakening, or steady monsoon backgrounds until landfall. Both of them are mature under the weakest WNPSM. In the SM cluster, the WNPSMI is always greater than 5 m s^{-1} during the seven-day period. The WNPSMI maintains above 11 m s^{-1} more than ten days before the Damrcy (0518) landfall, and the other four typhoons have the top four strongest WNPSMIs. In the MM cluster, the WNPSMI retains the sharpest increasing trend during the seven-day period. Their peak values show relatively few differences and rank in the second team. It is obvious that the characteristics of the temporal evolutions of the WNPSM before the LSTYs landfall are unique in each cluster, indicating that the classification here is reasonable.

4. Composite Analysis of the Classified LSTYs

From entering the SCS to landfall, most of the LSTYs take three days (Figure 1b). The monsoon peaks within 3 days before the TC landfall (Figure 2b) and the 3-day period is crucial to coastal citizens and the forecasting operation; thus, the 3-day period has been investigated in the rest of this paper. In order to obtain a more obvious contrast among the clusters, the unfiltered parameters are shown in the rest of the paper and the results have not changed.

4.1. Environmental Circulation

The potential destructiveness of a TC is not only related to the MSW, but also to the radial extent of the near-surface wind, namely the outer TC size. In this study, the outer TC size is represented by the radius of 9 m s^{-1} winds in ERA5, as recommended by Bian et al. [39]. Thus, near-surface wind fields are firstly investigated by the 10 m azimuthal-mean wind speeds for the three clusters (Figure 3). As shown in Figure 3, the LSTYs continued to intensify before landfall. A slow contraction of the wind radius is accompanied by the intensification of the LSTYs in all three clusters. There are few differences in the radius of MSW (~100 km). However, the outer TCs size shows a large difference among the three clusters. The TCs outer size is enlarged along with the enhancement of the TCs and monsoon intensity. The outer size in cluster WM, MM, and SM is 200–300 km, 300–400 km, and 350–600 km, respectively, indicating that the TCs size is closely related to the strength of the monsoon. Both of the two TCs in cluster WM experienced RI just before landfall, leading to the strongest landfall intensity (Figure 3a). Despite their strongest landfall intensity, the TCs still had the smallest horizontal scale in the weak monsoon background.

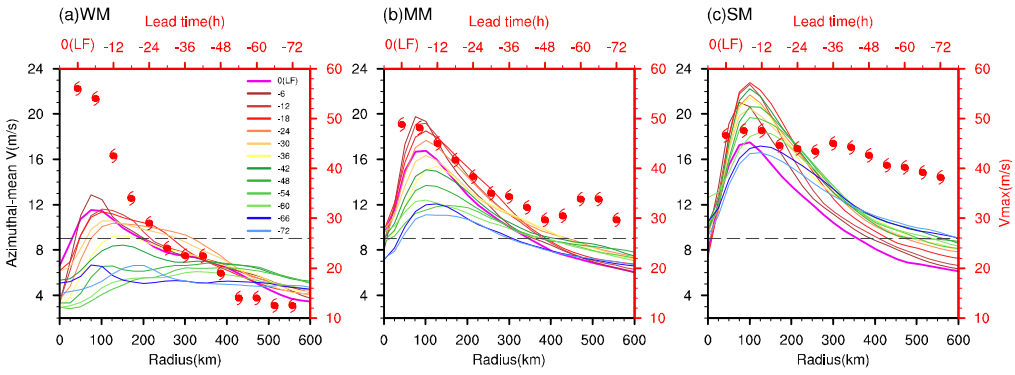


Figure 3. Dynamic composite of the 10 m azimuthal-mean wind speeds (solid lines, m s^{-1}) and typhoon intensity (the red typhoon labels, m s^{-1}) from 72 h before landfall to landfall (LF). (**a**) Cluster WM, (**b**) cluster MM, (**c**) and cluster SM. The horizontal dash lines reveal the 9 m s^{-1} 10 m wind speeds. The bottom, upper, left, and right axes indicate the distance from TC center, the lead hours before TC landing in SC, the 10 m azimuthal-mean wind speeds, and TC intensity, respectively. Information for wind speed (TC) should refer to the bottom and left (upper and right) axes. Negative values in label legends and the upper axis indicate the hours before TC landing in SC.

The middle- and low-level circulation during the LSTYs landfall is shown in Figure 4. In WM, the southwesterly was very weak and the low-level jet (LLJ) was absent, resulting in a rather weak water vapor transport to the typhoon. During the typhoon landfall process, the northern part of the typhoon was completely covered by the 588 dam (Figure 4d) due to the westward extension of the western North Pacific subtropical height (WNPSH), whereas the LLJ is prominent in cluster MM and extends further southward to -10° degrees (Figure 4b). Simultaneously, there was a remarkable water vapor belt to the south of the typhoon and the contour of 16 s^{-1} hPa^{-1} cm^{-1} stretches southward to (0, -10) (Figure 4e). However, the WNPSH was relatively stable during the typhoon landfall process. Along with the enhanced monsoon, the LLJ and water vapor channel not only extended southward to -10° degrees but they also stretched westward to -28° degrees 24 h before the typhoon's landfall (Figure 4c). Both the core of the LLJ and water vapor channel were further enhanced at the landfall time (Figure 4f). As for the WNPSH, it slightly shrunk eastward during the TC landfall. It is worth noting that the small vortex to the southeast of the typhoon was another immature TCs. As shown in Figure 4, the horizontal scale of the TCs cannot vigorously develop without the warm–wet southwesterly monsoon flow, which is consistent with the results of the near-surface wind fields in Figure 3. It is clear that the low-level circulation of the three types of LSTYs are totally different, indicated by their dynamic variations during the landfall processes and strength of the related systems. The aforementioned differences further demonstrate that the classification based on the seven-day period monsoon intensity is valid.

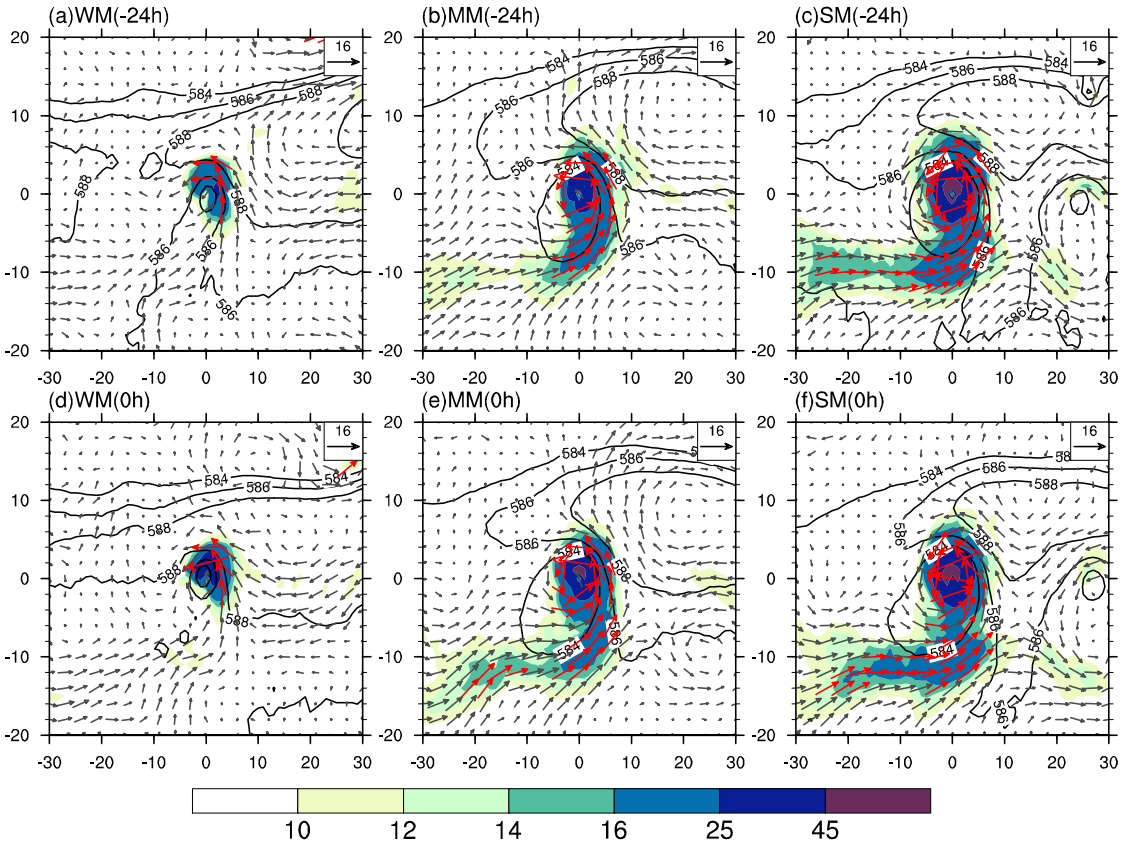


Figure 4. Composite of the 850 hPa wind (vector, m s^{-1}), water vapor flux (shaded, g s^{-1} hPa^{-1} cm^{-1}), and 500 hPa geopotential height (contour, dam) fields on (**a**–**c**) 24 h before landfall and landfall time (**d**–**f**) for cluster WM (**a**,**d**), MM (**b**,**e**), and SM (**c**,**f**), respectively. Red vectors indicate the low-level jet (wind speed $\geq$ 12 m s^{-1}). The origin points (0, 0) are typhoon centers. Positive (negative) coordinates denote the distance from typhoon center by degrees at northward (southward) and eastward (westward) direction.

A stronger upper-level outflow is usually followed by a heavier intensified TC. Therefore, the characteristics of upper-level conditions are revealed in Figure 5. In the summer half-year, the South Asia High (SAH) controls the upper troposphere, so the prevailing northeasterly winds are found over the typhoons (Figure 5). However, differences still exist in different monsoon intensities. In a weak monsoon background (Figure 5a,d), the SAH is weakest and the divergence in the upper level is not obvious over the typhoon's center. In the moderate monsoon situation, the SAH and divergence are the strongest (Figure 5b). The center of the SAH in MM is 12 (8) dam higher than that in weak (strong) monsoon background (Figure 5a–c). Relatively speaking, the center of the SAH locates the furthest to the northwest of the typhoon centers in cluster MM.

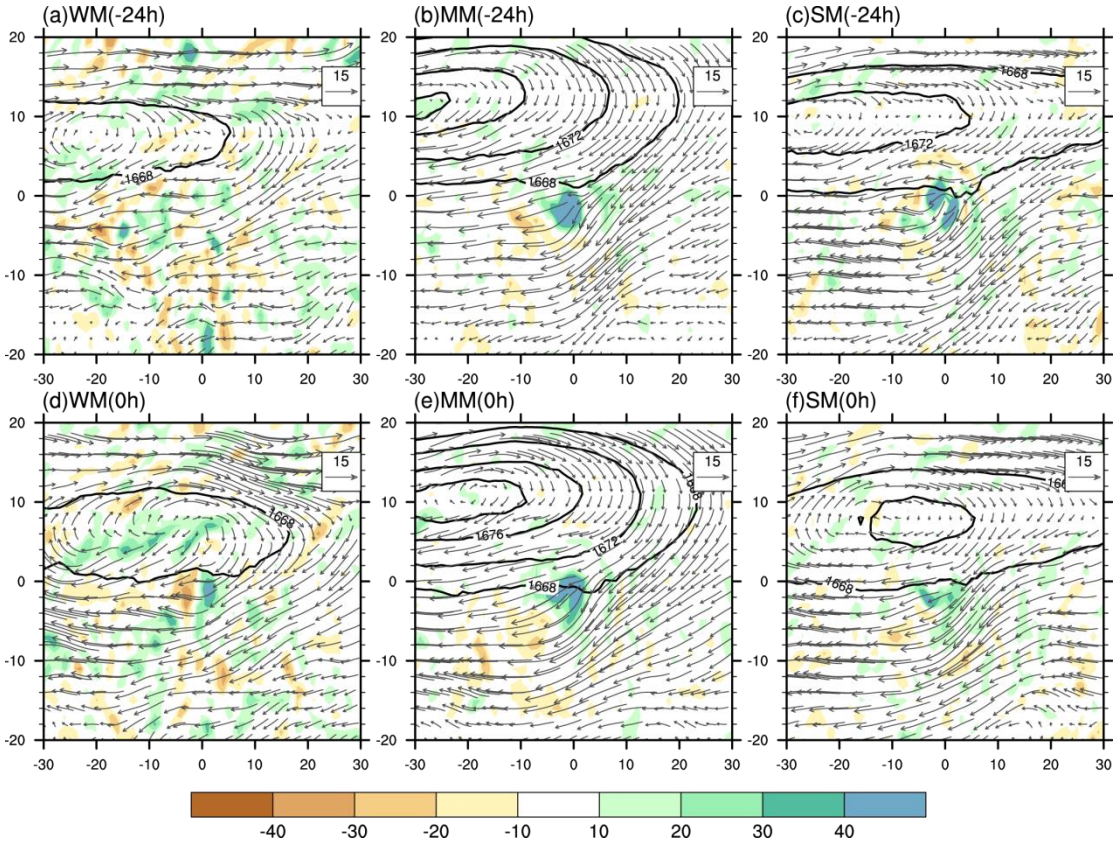


Figure 5. Same as in Figure 4, but for the 200 hPa wind fields (vector, m s^{-1}), geopotential height (contour, dam), and divergence (shaded, 10^{-6} s^{-1}).

In order to reveal differences in the vertical circulation for the three clusters, the corresponding meridional vertical circulation across the typhoon centers is shown in Figure 6. Only the circulation 12 h and 24 h before landfall are depicted here. In cluster WM (Figure 6a,d), the vertical upward motion mainly locates at the southern part of the TCs, and the center occurs at the middle troposphere. In the moderate monsoon background (Figure 6b,e), the vertical motion is enhanced in upper levels with the magnitude of 1.5 Pa s^{-1}. Compared with the weak monsoon, the upward motions gradually appear at the lower troposphere of the northern part of the TCs. The updraft air develops vigorously (>2 Pa s^{-1}) in cluster SM with the most intense monsoon (Figure 6c,f), especially at the southern part of the LSTYs. There are two upward centers at the lower and upper level (Figure 6c), respectively. The upward motion at the lower troposphere is much stronger than that of the upper level, which may be strongly related to the strong LLJ, as shown in Figure 4c. At the time of 24 h prior to landfall (Figure 6f), a broad vertical motion appears in strong monsoon situations and it extends southward to −4° degrees. There are

two ascending branches found at the southern part of the LSTYs and it is accompanied by the strongest ascending motion at the northern part of the TCs.

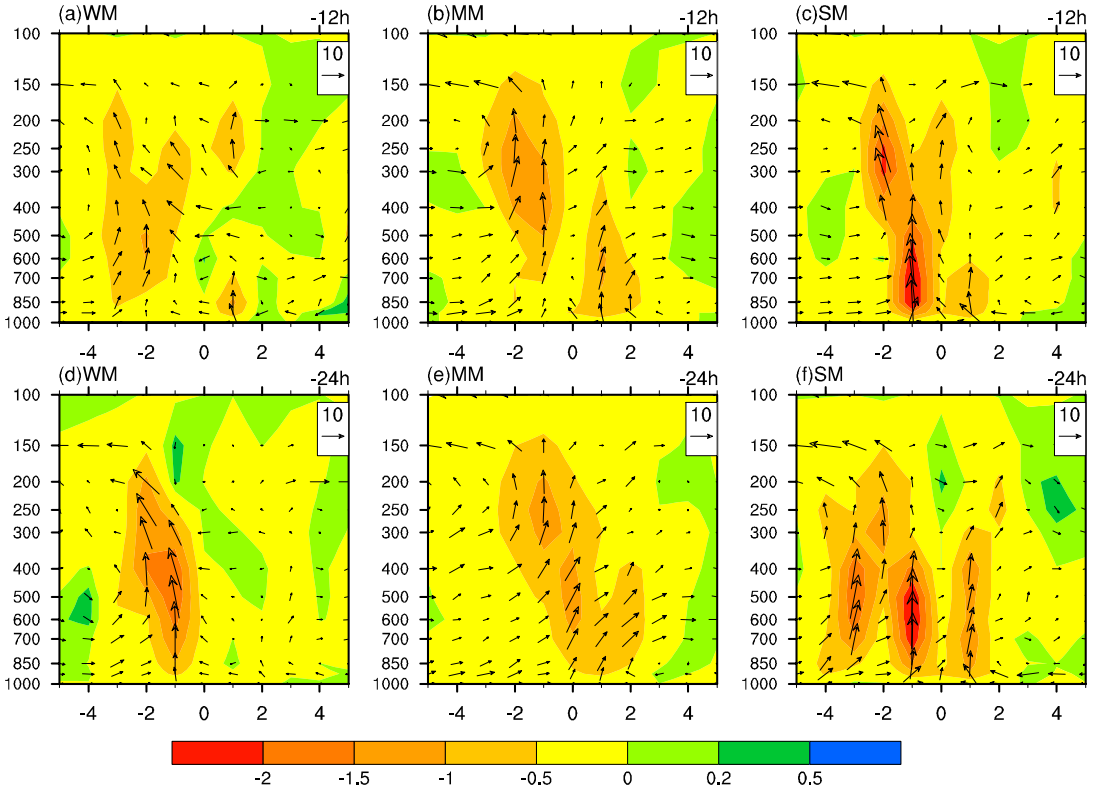


Figure 6. Composites of the meridional vertical circulation (vectors, m s^{-1}) and vertical speed (shaded, Pa s^{-1}) passing typhoon centers for three clusters at the monsoon peak time. (**a**–**c**) 12 h before landfall and (**d**–**f**) 24 h before landfall. (**a**,**d**) Cluster WM, (**b**,**e**) cluster MM, (**c**,**f**), and cluster SM.

4.2. Humidity and Thermal Structures

Water vapor is a very important factor affecting the development of a typhoon. The temporal evolutions of the lower-level water vapor are shown in Figure 7. Although all TCs in this study are above the intensity of STYs at landfall, the water vapor distributions among the three clusters are strongly related to the strength of the summer monsoon. In WM cases, the water vapor flux (Figure 7a) and divergence (Figure 7d) are almost absent at the southern quadrants and they are mainly in the northern part of the TCs. As for the strength, they are the weakest compared with the cluster MM and SM, and their enhancement only occurs near landfall. In the cluster MM, the water vapor flux of the southern branch is already stronger than the core in the cluster WM, though the strongest core still locates at the northern part (Figure 7b). The southern branch water vapor flux gradually extends southward to $-10°$ degrees at landfall (Figure 7b), which is accompanied by the rapid enhanced of the summer monsoon (Figure 2b). The water vapor convergence distributes symmetrically over both sides of the TCs and begins to intensify 66 h before landfall (Figure 7e). However, the monsoon maintains a relatively strong intensity for several days before landfall in the cluster SM (Figure 2b), and the water vapor flux (Figure 7c) and convergence (Figure 7f) are the strongest. The second enhancement of the convergence occurs at 48 h before landfall with the core above -15×10^{-4} kg m^{-2} s^{-1} (Figure 7f). It is worth noting that the meridional water vapor fluxes at the northern part are a concordant stronger than the southern branch in all three clusters (Figure 7a–c).

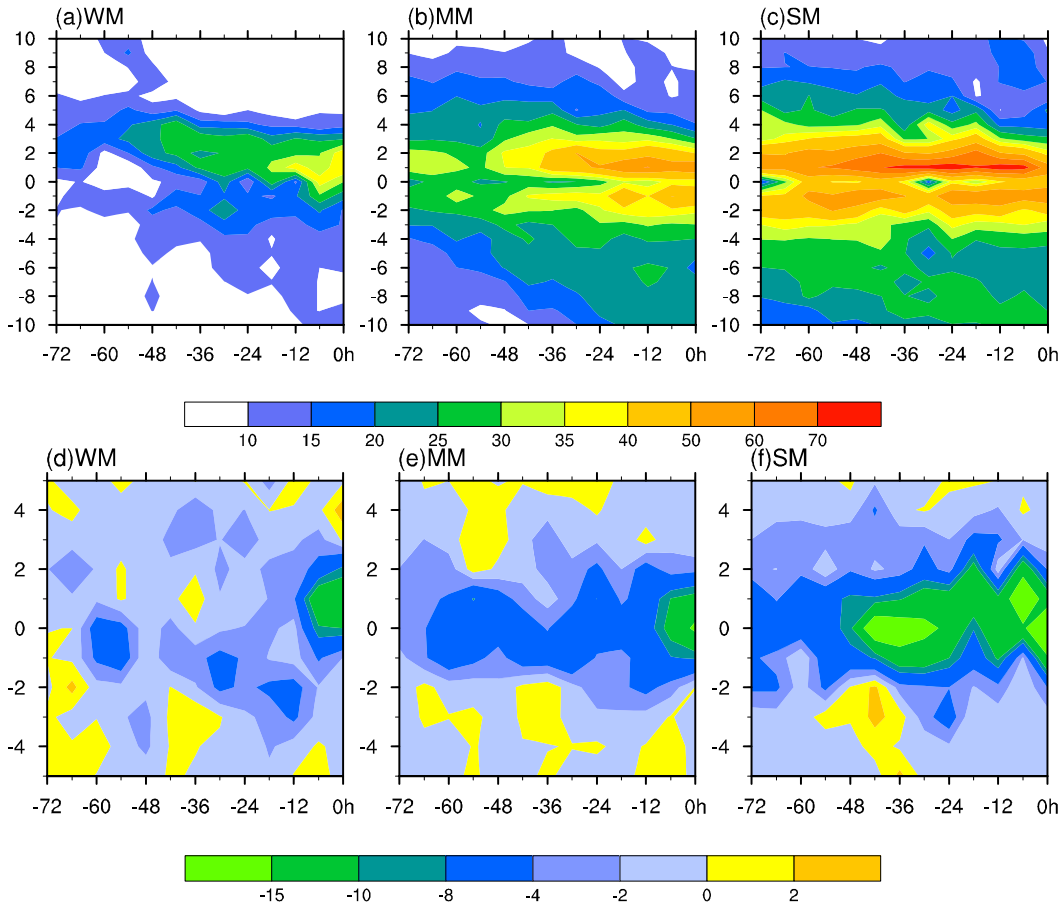


Figure 7. Dynamic composite of the meridional water vapor flux (**a**–**c**, g s^{-1} hPa^{-1} cm^{-1}) and water vapor flux divergence (**d**–**f**, 10^{-4} kg m^{-2} s^{-1}) passing typhoon centers at 925 hPa from 72 h before landfall to the landfall time. (**a**,**d**) Cluster WM, (**b**,**e**) cluster MM, (**c**,**f**), and cluster SM. Vertical and horizontal ordinates are degrees of latitude away from typhoon centers and hours before the LSTYs landfall (0 h).

The characteristics of the vertical structural of the humidity and temperature are depicted in Figure 8. First, the differences in the humidity and temperature between each grid value and the average value of the 5° × 5° box centered on the typhoon are calculated based on a certain layer. Then, warm-core and wet-core are obtained by the maximum value in the first step. It can be found that there are large differences in the wet cores and warm cores in the three clusters (Figure 8). In the cluster WM, the wet core was very weak and started to enhance until 12 h before landfall (Figure 8a) and it reached its peak value of about 2 g kg^{-1} at landfall at 700 hPa. The water vapor flux convergence peaked at 6 h before landfall at 925 hPa. In terms of the temporal variation, twice enhancements of the wet core were found in the cluster MM at 66 and 36 h before landfall (Figure 8b), respectively. Humidity in the vertical direction was strong as the 1 g kg^{-1} contour stretches upward to 400 hPa and the wet core was downward to 850 hPa. Several wet cores above 3 g kg^{-1} were found below 700 hPa (Figure 8c) as TCs moving westward in cluster SM. Humidity was further enhanced in the vertical direction. This is indicated by the contours of 2 g kg^{-1} and 1.5 g kg^{-1} extending upward to 600 and 500 hPa, respectively. The water vapor flux convergence at the lower level was further enhanced; it is more than two-fold that in the WM and was maintained more than 48 hours before landfall.

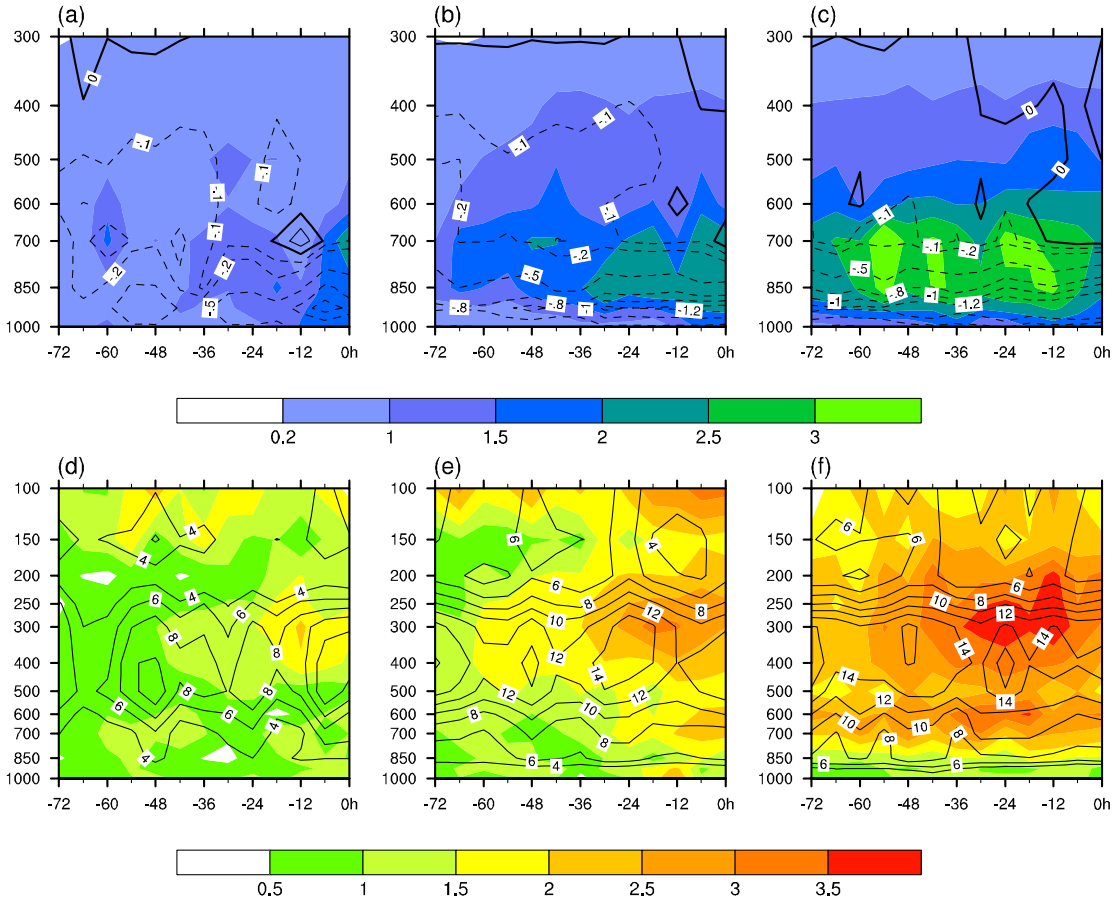


Figure 8. Same as in Figure 7, but for the vertical cross-section of wet (**a**–**c**, g kg^{-1}) and warm (**d**–**f**, K) core in shading. Contours in (**a**–**c**) and (**d**–**f**) are water vapor flux divergence (10^{-4} kg m^{-2} s^{-1}) and diabatic heating rate (K d^{-1}) averaged by the 5° × 5° grid box centered on typhoon, respectively.

The warm core is another one of the most important features of typhoons. It is mainly caused by the adiabatic warming of a subsidence in the eye region and diabatic heating of the latent heat released by precipitation. As shown in Figure 8d–f, the warm cores showed an increasing trend along with the enhancement of the summer monsoon in three clusters. The maximum warm core was found to be near 300 hPa, which is the same as a previous study [40]. The 2 K warm core was found 12 h before landfall in the cluster WM (Figure 8d). Additionally, the warm core was enhanced to 3 K in the cluster MM and a secondary warm heart of about 2 K was found at the low-level of 600–700 hPa at 12 h before landfall (Figure 8e). The upper- and low-level warm cores (>3.5 K) were further enhanced in the cluster SM (Figure 8f) and its low-level warm core retained company with the upper warm core for more than 60 h.

4.3. Interactions between Ocean and Typhoon

The supplementation of energy from the ocean to a typhoon is an important factor affecting the intensification of a typhoon. Wang et al. [41] claimed that TCs are hardly intensified when the SST is lower than 27 °C. As shown in Figure 9a, the SST is higher than 27 °C and most of the TCs travel over warm oceans (SST > 28 °C), indicating that the ocean provides favorable conditions for the development of LSTYs. In terms of the amplitude, the SSTs are different among the three clusters. The SST is the lowest in the cluster SM and highest in the cluster WM. Thirty hours before landfall, both the SST in the cluster MM and SM decrease. The phenomena may be ascribed to the TCs entering a colder offshore or SSTs cooling faster by the TCs in cluster MM and SM. On the contrary, the TCs in the

cluster WM enter into a warmer offshore or exert little impact on the SST cooling, thus the SST shows an increasing trend.

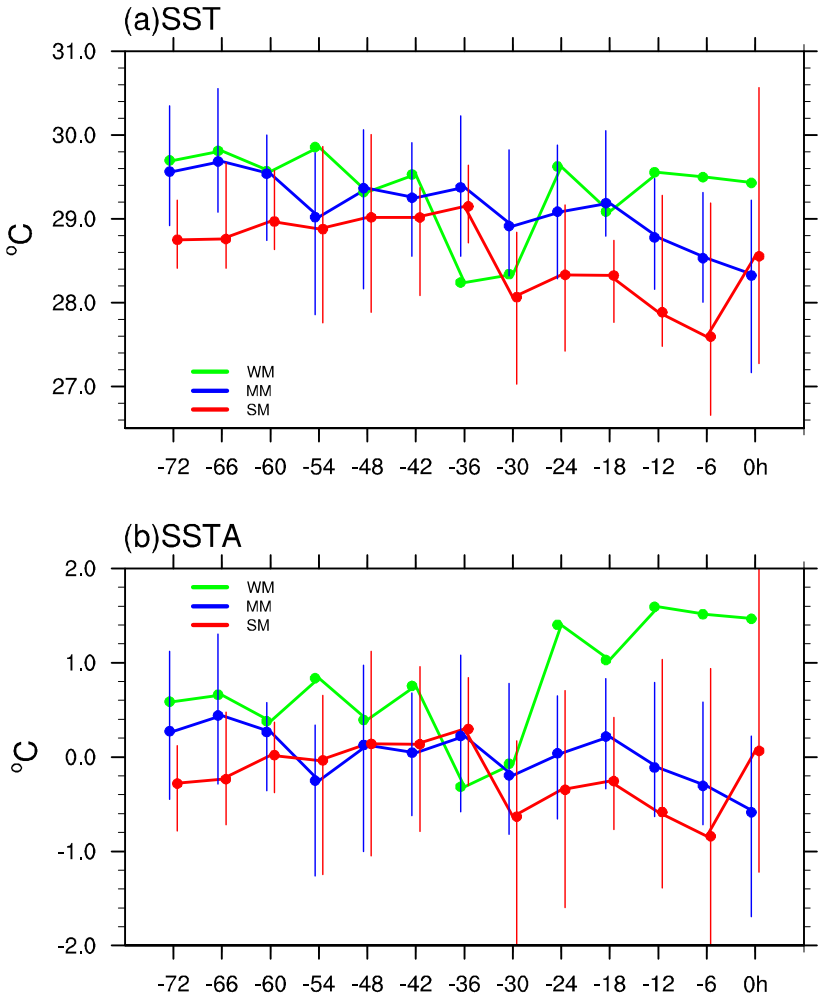


Figure 9. Temporal evolutions of the SST (**a**) and SSTA (**b**) in typhoon center for three clusters from 72 h before landfall to landfall. Vertical bars are the range temperature among each cluster. Units: °C.

The sea surface temperature anomaly (SSTA; Figure 9b) shows a similar trend compared with the SST. Though the SST in the three clusters is greater than 27 °C, the amplitudes of the SSTA are totally different. The SSTA is retained at an almost normal status during the TCs landfall in the cluster MM and SM. However, the disparity of the SSTA becomes larger one day before landfall. The SSTA increases significantly in the cluster WM the day before landfall and maintains at around 1.4 °C. This may be ascribed to TCs moving into the warmer-than-normal coastal ocean.

Due to large discrepancies of the SST and SSTA 24 h before landfall, the spatial distributions of the SST and SSTA at the landfall day and SST cooling have been depicted in Figure 10. It is clearly found that the SST is slightly higher in the cluster WM than those in the clusters MM and SM (Figure 10a–c) at the offshore ocean. Furthermore, the nearer to the offshore, the warmer SST is found in the cluster WM (Figure 10a), which coincides with Figure 9a. In terms of the SSTA, differences are also obvious among the three clusters. Cluster WM has the maximum SSTA, followed by the clusters MM and SM. Most of the coastal ocean is warmer than normal and the magnitude is about 1–2 °C in the cluster WM (Figure 10a), whereas a negative SSTA is found in the cluster MM and SM (Figure 10b,c) with the magnitude of −0.5 °C and −1 °C, respectively. SST cooling centers locate to the northern part of the TCs in three clusters (Figure 10d–f). The maximum cooling (about

−2 °C) occurs in the cluster SM, while the cooling strength in the clusters MM and WM is only about −1.5 °C. The weak cooling is one of the reasons that make the SSTA maintain a relatively high level in the cluster WM. The temperature profiles of the northern SCS (17–22° N, 111–120° E) have been checked by the pentad GODAS dataset. The subsurface ocean in cluster WM is warmer than the rest of the two clusters until ~300 m (figure not shown). The thicker warm-water layer in the upper ocean compensates the SST cooling to some extent [6].

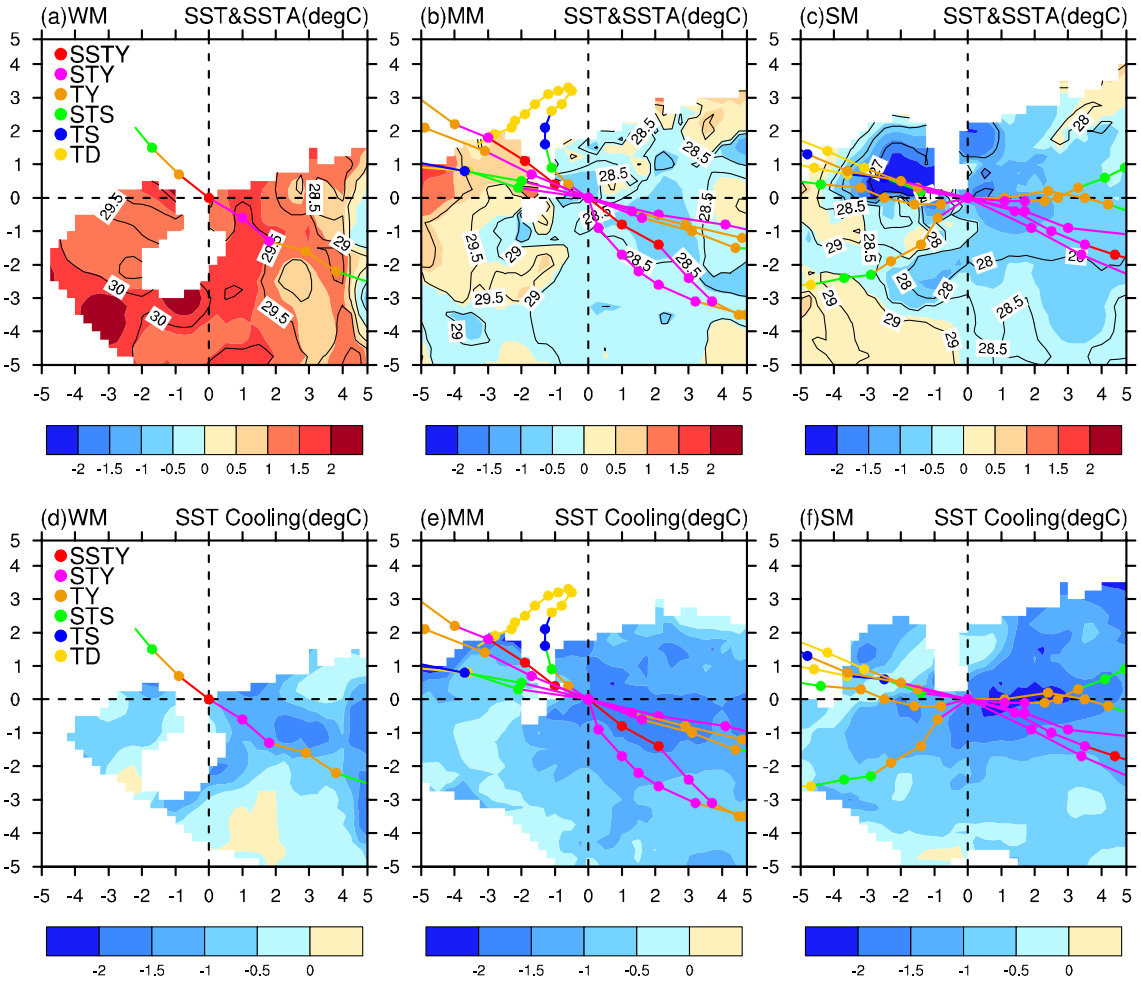


Figure 10. Dynamic composites of the SST (**a**–**c**, contour) and SSTA (**a**–**c**, shaded) at the landfall day and amplitudes of the SST cooling (**d**–**f**) at the offshore area. The corresponding TCs tracks are shown in curves and circles. The origin coordinates (0, 0) indicate the landfall position. Vertical and horizontal coordinates are the north–south and west–east direction in degrees, respectively. (**a**,**d**) Cluster WM, (**b**,**e**) cluster MM, and (**c**,**f**) cluster SM. Units: °C.

The ocean's energy supply (i.e., enthalpy heat flux, defined as the sum of sensible and latent heat fluxes) for the TCs' intensification is shown in Figure 11. It can be seen that there is a sharp gradient of the enthalpy heat flux in the cluster WM in the coastal ocean and it rapidly increases to 400 W m^{-2} near the landfall position (Figure 11a), which keeps in pace with the RI process near landfall (Figure 3a). On the contrary, the enthalpy heat flux in the clusters MM and SM shows little change over the offshore region (Figure 11b,c) and it is only a quarter of that in the cluster WM.

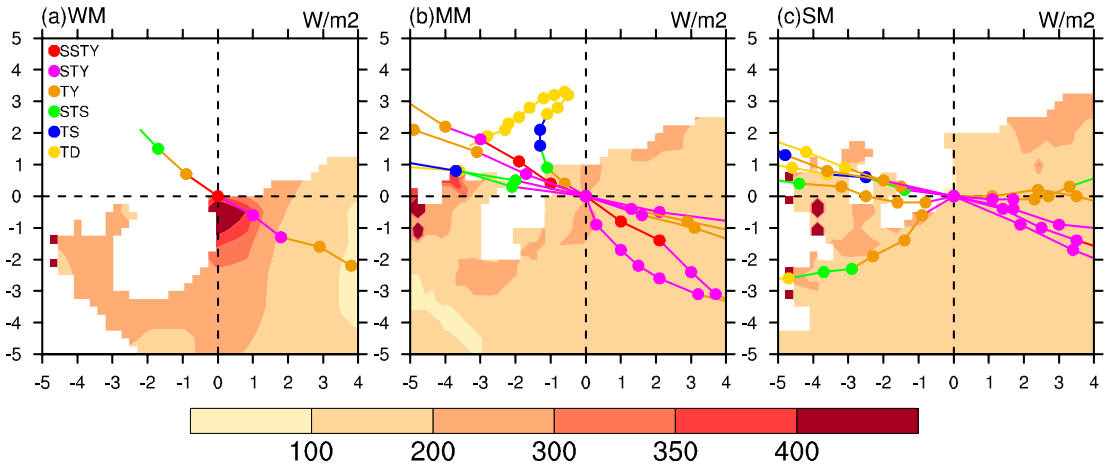


Figure 11. Same as in Figure 10, but for enthalpy heat flux. (**a**) Cluster WM, (**b**) cluster MM, (**c**) and cluster SM. Units: W m^{-2}.

For a longer time period, the ocean's energy supply for the LSTYs is also different among three clusters (Table 2). It can be seen that the averaged enthalpy heat flux in cluster WM is 239.02 W m^{-2}, and it surpasses the cluster MM (SM) by 63.46 (88.13) W m^{-2}. TCs travel fastest (6.60 m s^{-1}) in the cluster MM and slight slower (6.18 m s^{-1}) in cluster WM, whereas the TCs have a much slower traveling speed (5.37 m s^{-1}) in the cluster SM. The fast traveling speed contributes to suppressing the SST cooling [42], which partially reflects the relatively weak cooling magnitude in the clusters WM and MM (Figure 10d,e). TCs travel the longest (shortest) distance in the cluster MM (SM) for three days before landfall. However, even so, the cluster WM still has the biggest distance-integrated fluxes from the ocean due to its high averaged enthalpy heat flux. Because of the smallest averaged flux and shortest moving distance, it is not surprising that there is a much smaller energy supply for the cluster SM than the cluster MM and WM. These results suggest that TCs can reach the same intensity with a sufficiently high ocean energy flux supply, and it is not essential for a strong moisture and heat provision from the monsoon flow.

Table 2. Comparisons of the averaged flux, translation speed, moving distance, and distance-integrated flux for three cluster TCs in three days before landfall.

Cluster	Avg. Enthalpy Heat Flux (W m^{-2})	Translation Speed (m s^{-1})	Travelling Distance (km)	Distance-Integrated Flux (W m^{-2} × km)
WM	239.02	6.18	1489.59	2.86×10^5
MM	175.56	6.60	1642.20	2.50×10^5
SM	150.89	5.37	1261.82	1.71×10^5

Though all of the TCs investigated in this study are LSTYs, they have particular characteristics under strong and weak summer monsoon conditions. Their unique characteristics can be summarized with a conceptual model, as depicted in Figure 12. In a weak monsoon background (Figure 12a), both the warm and moist air transported to the typhoon from the monsoon flow and the upper-level divergence are feeble. Dynamical and water vapor conditions are averse to enlarge the size of the TC, resulting in a rather weak warm and wet core. The TCs mainly gain energy from the offshore warming ocean and then rapidly intensify before landfall. Whereas in a strong monsoon background (Figure 12c), there is plenty of warm–wet airflow trapped in the typhoon by the robust southwesterly monsoon flow. Fed by intense heat and moisture with the vigorous upward motions, the TCs develop strongly, with a large warm core and wet core in the upper and lower level, respectively. The summer monsoon also provides heat and moisture for typhoons in the moderate monsoon background (Figure 12b). However, the SAH is so strong that it to leads

to a powerful upper divergence, which provides favorable dynamical conditions for the intensification of the TCs. Temporal variations in the WNPSH during landfall are different, i.e., the westward stretch, which is almost unchanged, and the eastward retreat in cluster WM, MM, and SM, respectively.

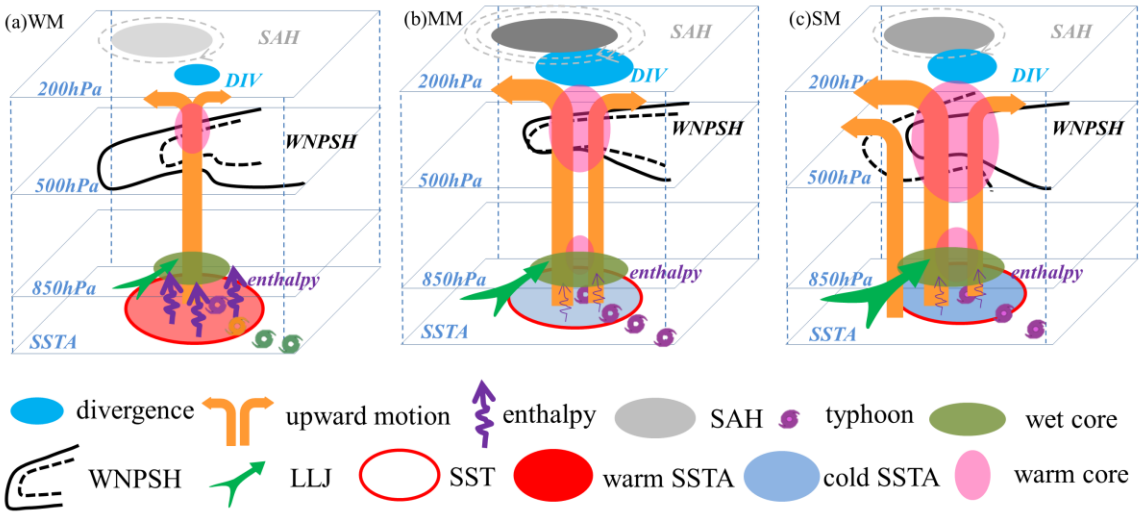


Figure 12. Schematic of the related element for three types of LSTYs in SC from surface to 200 hPa. (**a**) Cluster WM, (**b**) cluster MM, (**c**) cluster SM. Black solid and dash lines indicate the WNPSH at landfall time and 24 h before landfall, respectively.

5. Conclusions and Discussion

This study attempts to determine the influence of the summer monsoon on the LSTYs in SC. The thermal and dynamical characteristics of the LSTYs show great differences under different monsoon intensities. The dynamical and thermal factors, water vapor, and thermal structures of the LSTYs, and the related air–sea systems, are investigated by composite analysis. Different development patterns of the LSTYs supported by several potential factors are pointed out. The major results are summarized as follows:

Based on the strength of the WNPSMI, three types of monsoon backgrounds and the related LSTYs have been classified, i.e., as weak, moderate, and strong monsoons. The low-level jet is remarkably different among the three clusters, which leads to a significant difference in the water vapor transported to a typhoon.

Lacking the warm and moist monsoon flow which is involved in a typhoon, there is not enough water vapor in the cluster WM, leading to a feeble wet and warm core in the TC. However, a strong low-level wet core is found in strong monsoon conditions. Therefore, typhoons in the cluster SM intensify strongly, which is not only revealed by the largest horizontal size and vigorous upward motion, but also by the most intense upper and a secondary low-level warm core. The structures of the TCs in the cluster MM are similar to cluster SM but with differences in the intensity.

All of the TCs revealed in this study make landfall in SC with the intensity of an STY or SSTY, but the way the TCs develop into an STY are totally different. Despite being embedded in unfavorable atmospheric warm and wet conditions, the TCs still can reach a very intense level. It is mainly fed by the large energy supply from the offshore ocean. Therefore, both of the two TCs in the cluster WM are only rapidly intensified in the coastal ocean. On the contrary, the TCs in the cluster SM are not so strongly reliant on the ocean's energy supply. They can strongly intensify far away from the SC and maintain a high intensity for several days until landfall, which is mainly ascribed to the constantly strong summer monsoon flow. The development of the TCs in the cluster MM is more likely a combination effect from the atmosphere and ocean, i.e., both the monsoon flow and ocean energy supply are in moderate conditions. It is worth noting that the intense

upper-level divergence may play an auxiliary role in the cluster MM, though there is no further discussion of this topic in this paper. The clusters MM and SM account for a large proportion (11/13) and the monsoon flows are highly similar, but they differ in strength, indicating that the active monsoon background favors the TCs' intensification. However, there is a particular type of LSTYs (2/13) which can strongly intensify offshore when the monsoon flow is almost absent. The schematics of the related impacting systems for the three types of LSTYs are summarized. Knowing the dynamic variation in the LSTYs before landfall in SC is beneficial for the weather forecaster.

As mentioned above, there are several systems strongly interacting with the LSTYs in SC, including the SAH, WNPSH, LLJ, WNPSM, and SST. Though composite analysis has been conducted here to obtain the characteristics of the three types LSTYs related to the monsoon intensity, the typhoons' landfall intensity is very complicated. Due to the small sample size of the LSTYs in SC and the fact that uncertainty exists, other regions could be reexamined. On the other hand, though the circulation of TCs has been removed when calculating WNPSMI, the TCs' feedback on monsoons is also very important and it has not yet been solved here. In the future, coastal regions still face a serious impact from an intense landfall typhoon under global warming. Potential physical processes, the relative importance of the oceanic response, and system coupling mechanisms for typhoons' landfall intensity are all in need of a further investigation.

Author Contributions: Conceptualization, Z.X. and C.Y.; methodology, Z.X.; software, Z.X.; validation, Z.X. and C.Y.; formal analysis, Z.X. and C.Y.; writing—original draft preparation, Z.X.; writing—review and editing, C.Y.; visualization, Z.X.; supervision, C.Y.; funding acquisition, C.Y. All authors have read and agreed to the published version of the manuscript.

Funding: This work was sponsored by the National Natural Science Foundation of China (Grants Nos. 41465003), the Innovation Group of Southern Marine Science and Engineering Guangdong Laboratory (Zhuhai) (Grant 311021001), Guangxi Key Research and Development Program (GuiKeAB22035016 and GuiKeAB21196041), and Guangxi Meteorological Scientific Research Program (Guiqike 2021ZL05).

Institutional Review Board Statement: Not applicable.

Informed Consent Statement: Not applicable.

Data Availability Statement: The reanalysis data in this paper were downloaded from ERA5 (https://cds.climate.copernicus.eu/#!/search?text=ERA5&type=dataset, accessed on 12 July 2020). The TC best-track data were obtained from the Shanghai Typhoon Institute of the China Meteorological Administration (https://tcdata.typhoon.org.cn/en/index.html, accessed on 1 May 2022).

Conflicts of Interest: The authors declare no conflict of interest.

References

1. Huang, W.K.; Wang, J.J. Typhoon damage assessment model and analysis in Taiwan. *Nat. Hazards* **2015**, *79*, 497–510. [CrossRef]
2. Webster, P.J. Myanmar's deadly daffodil. *Nat. Geosci.* **2008**, *1*, 488–490. [CrossRef]
3. Webersik, C.; Esteban, M.; Shibayama, T. The economic impact of future increase in tropical cyclones in Japan. *Nat. Hazards* **2010**, *55*, 233–250. [CrossRef]
4. Pielke, R.A.; Gratz, J.; Landsea, C.W.; Collins, D.; Saunders, M.A.; Musulin, R. Normalized hurricane damage in the United States: 1900–2005. *Nat. Hazards Rev.* **2008**, *9*, 29–42. [CrossRef]
5. Takagi, H. Statistics on typhoon landfalls in Vietnam: Can recent increases in economic damage be attributed to storm trends? *Urban Clim.* **2019**, *30*, 100506. [CrossRef]
6. Lin, I.I.; Pun, I.F.; Lien, C.C. "Category-6" supertyphoon Haiyan in global warming hiatus: Contribution from subsurface ocean warming. *Geophy. Res. Lett.* **2014**, *41*, 8547–8553. [CrossRef]
7. Zhang, X.H.; Duan, Y.H.; Wang, Y.Q.; Wei, N.; Hu, H. A high-resolution simulation of supertyphoon Rammasun (2014) Part I: Model verification and surface energetics analysis. *Adv. Atmos. Sci.* **2017**, *34*, 757–770. [CrossRef]
8. Chen, G.M.; Zhang, X.P.; Cao, Q.; Zeng, Z.H. Evaluation of forecast performance for Super Typhoon Lekima in 2019. *Front. Earth Sci.-PRC* **2021**, *16*, 1–17. [CrossRef]
9. Leroux, M.D.; Wood, K.; Elsberry, R.L.; Cayanan, E.O.; Hendricks, E.; Kucas, M.; Otto, P.; Rogers, R.; Sampson, B.; Yu, Z.F. Recent advances in research and forecasting of tropical cyclone track, intensity, and structure at landfall. *Trop. Cyclone Res. Rev.* **2018**, *7*, 85–105.

10. Wang, Q.; Xu, Y.L.; Wei, N.; Wang, S.; Hu, H. Forecast and service Performance on rapidly intensification process of typhoons Rammasun (2014) and Hato (2017). *Trop. Cyclone Res. Rev.* **2019**, *8*, 18–26. [CrossRef]
11. Emanuel, K.A. Downscaling CMIP5 climate models shows increased tropical cyclone activity over the 21st century. *Proc. Natl. Acad. Sci. USA* **2013**, *110*, 12219–12224. [CrossRef] [PubMed]
12. Tsou, C.H.; Huang, P.Y.; Tu, C.Y.; Chen, C.T.; Tzeng, T.P.; Cheng, C.T. Present simulation and future typhoon activity projection over western North Pacific and Taiwan/east coast of China in 20-km HiRAM climate model. *Terr. Atmos. Ocean Sci.* **2016**, *27*, 687–703. [CrossRef]
13. Chen, J.L.; Tam, C.Y.; Cheung, K.; Wang, Z.Q.; Murakami, H.; Lau, N.C.; Garner, S.T.; Xiao, Z.N.; Choy, C.W.; Wang, P. Changing impacts of tropical cyclones on East and Southeast Asian inland regions in the past and a globally warmed future climate. *Front. Earth Sci.* **2021**, *9*, 769005. [CrossRef]
14. Knapp, K.R.; Kruk, M.C.; Levinson, D.H.; Diamond, H.J.; Neumann, C.J. The International Best Track Archive for Climate Stewardship (IBTrACS). *Bull. Amer. Meteor. Soc.* **2010**, *91*, 363–376. [CrossRef]
15. Liu, K.S.; Chan, J.C. Recent increase in extreme intensity of tropical cyclones making landfall in South China. *Clim. Dyn.* **2020**, *55*, 1059–1074. [CrossRef]
16. Mei, W.; Xie, S.P. Intensification of landfalling typhoons over the northwest Pacific since the late 1970s. *Nat. Geos.* **2016**, *9*, 753–757. [CrossRef]
17. Guan, S.D.; Li, S.Q.; Hou, Y.J.; Hu, P.; Liu, Z.; Feng, J.Q. Increasing threat of landfalling typhoons in the western North Pacific between 1974 and 2013. *Int. J. Appl. Earth Obs.* **2018**, *68*, 279–286. [CrossRef]
18. Yao, C.; Xiao, Z.X.; Yang, S.; Luo, X.L. Increased severe landfall typhoons in China since 2004. *Int. J. Climatol.* **2021**, *41*, E1018–E1027. [CrossRef]
19. Chen, L.S.; Xu, Y.L. Review of typhoon very heavy rainfall in China. *Meteor. Environ. Sci.* **2017**, *40*, 3–10. (In Chinese)
20. Chen, T.C.; Wang, S.Y.; Yen, M.C.; Gallus, W.A. Role of the monsoon gyre in the interannual variation of tropical cyclone formation over the western North Pacific. *Wea. Forecasting* **2004**, *19*, 776–785. [CrossRef]
21. Liang, J.; Wu, L.G.; Gu, G. Rapid weakening of tropical cyclones in monsoon gyres over the western North Pacific. *J. Climate* **2018**, *31*, 1015–1028. [CrossRef]
22. Chen, Z.Q.; Chen, L.S.; Li, Y. Interaction between landfalling tropical cyclone and summer monsoon with influences on torrential rain. *J. Appl. Meteor. Sci.* **2012**, *23*, 660–671. (In Chinese)
23. Chang, Y.L.; Yeh, H.C.; Liu, G.R. Monsoon effect simulation on typhoon rainfall potential-Typhoon Morakot (2009). *Terr. Atmos. Ocean. Sci.* **2017**, *28*, 11–21. [CrossRef]
24. Zhou, Y.S.; Wu, T.Y. Composite analysis of precipitation intensity and distribution characteristics of western track landfall typhoons over China under strong and weak monsoon conditions. *Atmos. Res.* **2019**, *225*, 131–143. [CrossRef]
25. Wu, T.Y.; Zhou, Y.S.; Wang, Y.Q.; Liang, L.; Han, F.R.; Lu, X. Comparative analysis of precipitation characteristics of the westward typhoon cases "Bilis" and "Sepat" during landfall under different monsoon intensities. *Chinese J. Atmos. Sci.* **2021**, *45*, 1173–1186. (In Chinese)
26. Xiao, Z.X.; Yao, C.; Luo, X.L.; Sun, H.M. A comparative study on the offshore intensification of supertyphoon Rammasun (2014) and typhoon Rumbia (2013): The role of summer monsoon. *Asia-Pac. J. Atmos. Sci.* **2021**, *57*, 405–420. [CrossRef]
27. Wei, X.W.; Wu, Q.T.; Chen, M.; Wu, H.; Li, X.H. The relationship between the offshore intensification of super typhoon Rammasun and low-frequency vapor transportation and its precedent signal. *J. Trop. Meteor.* **2017**, *33*, 267–272. (In Chinese)
28. Chen, X.M.; Wang, Y.Q.; Zhao, K.; Wu, D. A numerical study on rapid intensification of typhoon Vicente (2012) in the South China Sea. Part I: Verification of simulation, storm-scale evolution, and environmental contribution. *Mon. Wea. Rev.* **2017**, *145*, 877–898. [CrossRef]
29. Hersbach, H.; Bell, B.; Berrisford, P.; Hirahara, S.; Horányi, A.; Muñoz-Sabater, J.; Nicolas, J.; Peubey, C.; Radu, R.; Schepers, D.; et al. The ERA5 global reanalysis. *Quart. J. Roy. Meteor. Soc.* **2020**, *146*, 1999–2049. [CrossRef]
30. Reynolds, R.W.; Smith, T.M.; Liu, C.Y.; Chelton, D.B.; Casey, K.S.; Schlax, M.G. Daily high-resolution-blended analyses for sea surface temperature. *J. Climate* **2007**, *20*, 5473–5496. [CrossRef]
31. Gray, W.M. Recent advance in tropical cyclone research from rawnsonde composite analysis. In *World Meteorological Organization Programme on Research in Tropical Meteorology*; WMO Technic Report; Colorado State University: Fort Collins, CO, USA, 1981; 407p.
32. Li, Y.; Chen, L.S.; Wang, J.Z. The diagnostic analysis on the characteristics of large scale circulation corresponding to the sustaining and decaying of tropical cyclone after it's landfall. *Acta Meteor. Sinica* **2004**, *62*, 167–179. (In Chinese)
33. Wang, B.; Wu, R.; Lau, K.M. Interannual variability of the Asian summer monsoon: Contrasts between the Indian and the western North Pacific–East Asian monsoons. *J. Climate* **2001**, *14*, 4073–4090. [CrossRef]
34. Duchon, C.E. Lanczos filtering in one and two dimensions. *J. Appl. Meteor.* **1979**, *18*, 1016–1022. [CrossRef]
35. Li, J.; Sun, L.; Yang, Y.; Cheng, H. Accurate evaluation of sea surface temperature cooling induced by typhoons based on satellite remote sensing observations. *Water* **2020**, *12*, 1413. [CrossRef]
36. Ying, M.; Zhang, W.; Yu, H.; Lu, X.Q.; Feng, J.X.; Fan, Y.X.; Zhu, Y.T.; Chen, D.Q. An overview of the China Meteorological Administration tropical cyclone database. *J. Atmos. Ocean. Tech.* **2014**, *31*, 287–301. [CrossRef]
37. Wang, B.; Zhou, X. Climate variation and prediction of rapid intensification in tropical cyclones in the western North Pacific. *Meteorol. Atmos. Phys.* **2008**, *99*, 1–16. [CrossRef]
38. Hartigan, J.A.; Wong, M.A. A K-means clustering algorithm. *Appl. Stat.* **1979**, *28*, 100–108. [CrossRef]

39. Bian, G.F.; Nie, G.Z.; Qiu, X. How well is outer tropical cyclone size represented in the ERA5 reanalysis dataset? *Atmos. Res.* **2021**, *249*, 105339. [CrossRef]
40. Wei, Y.Z.; Xu, J.M. Retrieval of atmospheric temperature from NOAA-AMSU and its application in tropical cyclone analysis. *J. Nanjing Inst. Meteor.* **2005**, *28*, 522–529. (In Chinese)
41. Wang, Y.Q.; Rao, Y.J.; Tan, Z.M.; SchÖnemann, D. A statistical analysis of the effects of vertical wind shear on tropical cyclone intensity change over the western North Pacific. *Mon. Wea. Rev.* **2015**, *143*, 3434–3452. [CrossRef]
42. Price, J.F.; Sanford, T.B.; Forristall, G.Z. Forced stage response to a moving hurricane. *J. Phys. Oceanogr.* **1994**, *24*, 233–260. [CrossRef]

Disclaimer/Publisher's Note: The statements, opinions and data contained in all publications are solely those of the individual author(s) and contributor(s) and not of MDPI and/or the editor(s). MDPI and/or the editor(s) disclaim responsibility for any injury to people or property resulting from any ideas, methods, instructions or products referred to in the content.